(Running title:) Aldolase microcompartmentation in Arabidopsis guard cells

(Title:) Microcompartmentation of cytosolic aldolase in Arabidopsis by interaction with the actin cytoskeleton

Constantine Garagounis[1,4], Kalliopi-Ioanna Kostaki[2], Tim J. Hawkins[3], Ian Cummins[3], Mark D. Fricker[1], Patrick J. Hussey[3], Alistair M. Hetherington[2] and Lee J. Sweetlove[1]

[1]Department of Plant Sciences, University of Oxford, South Parks Road, Oxford OX1 3RB, UK

[2]School of Biological Sciences, University of Bristol, Life Sciences Building, 24 Tyndall Avenue, Bristol BS8 1TQ, UK

[3]School of Biological and Biomedical Sciences, Durham University, South Road, Durham, DH1 3LE, UK

[4]Corresponding author: kgkaragkounis@bio.uth.gr;

Highlight:

Microcompartmentation is a form of cellular organisation caused by the interaction of proteins with cellular structures and endomembranes. We show that a cytosolic isoform of the enzyme aldolase is microcompartmented in Arabidopsis guard cells by interaction with the actin cytoskeleton.

Abstract

Evidence is accumulating for molecular microcompartments formed when proteins interact in localised domains with the cytoskeleton, organelle surfaces, and intracellular membranes. To understand the potential functional significance of protein microcompartmentation in plants, we studied the interaction of the glycolytic enzyme fructose bisphosphate aldolase with actin in *Arabidopsis thaliana*. Homology modeling of a major cytosolic isoform of aldolase, FBA8,

suggested that the tetrameric holoenzyme has two actin binding sites and could therefore act as an actin-bundling protein, as was reported for animal aldolases. This was confirmed by *in vitro* measurements of an increase in viscosity of F-actin polymerized in the presence of recombinant FBA8. Simultaneously, interaction with F-actin caused non-competitive inhibition of aldolase activity. We did not detect co-localisation of an FBA8-RFP fusion protein, expressed in an *fba8*-knockout background, with the actin cytoskeleton using confocal laser-scanning microscopy. However, we did find evidence for a low level of interaction using FRET-FLIM analysis of FBA8-RFP co-expressed with the actin-binding protein GFP-Lifeact. Furthermore, knockout of FBA8 caused minor alterations of guard cell actin cytoskeleton morphology and resulted in a reduced rate of stomatal closure in response to decreased humidity. We conclude that cytosolic aldolase can be microcompartmented *in vivo* by interaction with the actin cytoskeleton and may subtly modulate guard cell behavior as a result.

Keywords: actin-binding, actin-bundling, aldolase, co-localisation, guard cell actin, guard cell metabolism, microcompartmentation;

Abbreviations list: ABA: abscisic acid, CLSM: confocal laser-scanning microscopy, FBA: fructose bisphosphate aldolase, F1,6-BP: fructose 1,6-bisphosphate, FRET-FLIM: Forster resonance energy transfer-fluorescence lifetime imaging microscopy, ROI: region of interest;

Introduction

Microcompartmentation is the phenomenon where soluble proteins have a non-homogeneous distribution within a single, membrane-bounded, sub-cellular compartment, typically through interaction of proteins with intracellular membranes or other cellular structures such as the cytoskeleton (Hudder *et al.*, 2003; Gierasch and Gershenson, 2009) and through liquid phase separation (Feric *et al.*, 2016). It remains unclear how this higher-level organization affects cell function, but there is some evidence that dynamic microcompartmentation

60 plays a regulatory role in both metabolism and intracellular signaling (Sweetlove
61 and Fernie, 2013). For example, glycerol phosphate dehydrogenase and various
62 glycolytic enzymes locate to actin-rich regions of the cell in fly muscle. Knocking
63 out this muscle-specific isoform of glycerol phosphate dehydrogenase led to a
64 flightless fly phenotype and also caused other glycolytic enzymes to become
65 uniformly distributed (Wojtas *et al.*, 1997; Sullivan, 2003). In HeLa cells,
66 enzymes involved in the synthesis of purines co-localized in distinct punctate
67 bodies, which were themselves co-localized with the microtubule cytoskeleton
68 when cells were grown on purine-depleted media, but had a uniform cytosolic
69 distribution when cells were grown in the presence of exogenous purines (An *et*
70 *al.*, 2008; An *et al.*, 2010). Both these examples illustrate how specific metabolic
71 pathways may be rapidly modulated via reversible enzyme
72 microcompartmentation. Additionally, recent theoretical models suggest that
73 microcompartmentation of enzymes by association with the tubulin cytoskeleton
74 may be used to integrate various metabolic pathways with other ongoing cellular
75 processes, thereby linking metabolic regulation with the current cell status (Olah
76 *et al.*, 2015).
77
78 In plants there are several known instances of microcompartmentation of
79 enzymes, including association of enzymes with microtubules (Chuong *et al.*,
80 2004) and actin (Holtgrawe *et al.*, 2005; Wojtera-Kwiczor *et al.*, 2012),
81 association of glycolytic enzymes with the surface of organelles (Giege *et al.*,
82 2003; Balasubramanian *et al.*, 2007; Graham *et al.*, 2007; Atteia *et al.*, 2009;
83 Huang *et al.*, 2009) or other intracellular membranes (Barkla *et al.*, 2009), and
84 association of enzymes of secondary metabolism with the cytosolic face of the ER
85 (Hrazdina and Wagner, 1985; Moller, 2010). In several of these examples, a role
86 in metabolic regulation has been suggested, either through the facilitation of
87 metabolite channeling between sequential enzymes (Graham *et al.*, 2007) or by
88 controlling reaction products of low-specificity enzymes (Moller, 2010).
89
90 To further investigate the role of enzyme microcompartmentation in
91 plants, we analysed the localization of a cytosolic isoform, AtFBA8 (encoded by
92 the *At3g52930* gene), of the glycolytic enzyme aldolase in Arabidopsis. Aldolase

93 (EC 4.1.2.13) is the fourth enzyme of the Embden-Meyerhof-Parnas glycolytic
94 pathway and mediates cleavage of fructose 1,6-bisphosphate (F1,6-BP) into
95 glyceraldehyde 3-phosphate and dihydroxyacetone phosphate. AtFBA8 is the
96 most abundantly expressed isoform of aldolase in Arabidopsis according to
97 publicly available microarray data (Hruz *et al.*, 2008). Previous work has
98 provided *in vitro* evidence showing aldolase is able to associate with the
99 mitochondrial surface in Arabidopsis cell cultures and potato tubers (Giege *et al.*,
100 2003; Graham *et al.*, 2007), to interact with actin in yeast-two-hybrid
101 experiments and co-sedimentation assays (Holtgrawe *et al.*, 2005; Wojtera-
102 Kwiczor *et al.*, 2012), and to co-immunoprecipitate with actin when using an
103 anti-aldolase antibody (Graham, 2007). However, the functional significance of
104 the aldolase-actin interaction has not been determined. Thus, we first
105 investigated the interaction of aldolase FBA8 with actin *in vitro* to assess
106 potential reciprocal functional effects that these two proteins might exert on
107 each other. We then assessed the occurrence of aldolase microcompartmentation
108 with actin *in vivo* using microscopy and finally determined potential functions of
109 this interaction using genetic approaches.

110 **Materials and Methods**

111

112 The aldolase *At3g52930* sequence was retrieved from the TAIR database.
113 Human (PAN P04075) and rabbit muscle (PAN P00883) aldolase protein
114 sequences and actin sequences P68133 and P68135 from human and rabbit
115 muscle, respectively, were aligned using Clustal Omega and LALIGN on the EMBL
116 website (ebi.ac.uk). Homology modeling was carried out using the Swiss-
117 PdbViewer DeepView, version 4.0.1, (Guex and Peitisch, 1997). The crystal
118 structure of rabbit muscle aldolase (RCSB PDB reference: 3DFQ) was used as a
119 template and the resulting model structure of Arabidopsis aldolase FBA8 was
120 modified in RasMol (Sayle and Milner-White, 1995) to mark residues of interest.

121

122 Chemicals and enzymes were purchased from Sigma Aldrich (St. Luis, MO,
123 USA). Rabbit muscle actin (catalogue number AKL99) was purchased from
124 Denver Cytoskeleton Inc. (Denver, CO, USA). *Arabidopsis thaliana* ecotype

125 Columbia-0 (Col-0) was used as a wild type control and was the basic genetic
126 background for all other plant lines used in this work. Salk T-DNA insertion lines
127 for FBA8:, Salk_124383 (*fba8-1)*, SALK_058908 (*fba8-2*), and SALK_007216
128 (*fba8-3*)*)* were ordered from the Nottingham Arabidopsis Stock Centre (NASC).
129 Unless specified otherwise, plants were germinated and grown on 0.8% (w/v)
130 agar plates supplemented with half-strength Murashige-Skoog (MS) salts
131 (Duchefa Biochemie, Haarlem, Netherlands) and 1% (w/v) sucrose for up to 10
132 days before transfer to 3:1 (v/v) compost:vermiculite mixture. Growth
133 conditions were 16/8hrs, light/dark at 22-23°C. *Nicotiana tabacum* cultivar
134 "Little Havana" and *Nicotiana benthamiana* were grown at 25°C 16/8hrs,
135 light/dark on 3:1 (v/v) compost:vermiculite.
136
137 Genomic DNA from Arabidopsis tissues was extracted by grinding tissue
138 under liquid N_2, adding DNA-extraction buffer [200mM Tris-HCl pH7.5, 250mM
139 NaCl, 25mM ethylene-diamine tetra-acetic acid, (EDTA) and 0.5% (w/v) sodium-
140 dodecyl sulfate (SDS)] followed by isopropanol precipitation. DNA concentration
141 was measured by Nanodrop (Thermo Fischer). RNA was extracted from mature
142 Arabidopsis leaves using the TRIzol® reagent from (Life Technologies, Thermo-
143 Fischer) following the manufacturer's instructions. Resulting RNA was treated
144 with DNase I (Fermentas). Reverse transcription of DNase-treated RNA was
145 carried out using the M-MLV reverse transcription kit and protocol from Sigma-
146 Aldrich with an oligo-deoxythymidine primer. PCRs on resulting cDNA were
147 carried out as described below with primers targeting a fragment of the
148 ubiquitin-10 transcript and the full-length aldolase FBA8 (At3g52930) transcript
149 (Supplementary Table S1).
150
151 PCR was carried out using Megamix Blue (Microzone Ltd., UK) according
152 to the manufacturers instructions (Supplementary Table 1 for primer pairs and
153 annealing temperatures). PCRs for sub-cloning of the aldolase coding sequence
154 (CDS) were carried out using Phusion High-Fidelity DNA polymerase (Thermo-
155 Fischer, Waltham, MA, USA). The RFP CDS was PCR-amplified from the
156 pUB:GW:RFP vector (Grefen *et al.*, 2010). For expression in *Pichia pastoris,* the
157 aldolase CDS was sub-cloned into the expression vector, pPICZαB (Invitrogen,

158 Carlsbad, CA, USA) using the PstI and XbaI restriction sites. The FBA8 CDS was
159 cloned in frame with the N-terminal secretion peptide and included a stop codon.
160 For expression of aldolase in plant cells, the aldolase CDS was sub-cloned into
161 binary vectors pUB:GW:RFP and pUB:RFP:GW described in (Grefen *et al.*, 2010)
162 to generate N- and C-terminal fusions of aldolase with mRFP1. The free RFP CDS
163 was cloned into the pUB:GW vector (Grefen *et al.*, 2010). Orientation and
164 sequence of the inserts in all of the generated plasmids was verified by
165 restriction digest and DNA sequencing. The GFP:Lifeact (GFP6) construct was
166 made in the pMDC43 binary vector (Deeks *et al.*, 2010). The free GFP (roGFP2)
167 construct (Schwarzlander *et al.*, 2009) was donated by Dr. Markus
168 Schwarzlander (University of Bonn, Germany).
169
170 Wild type *Pichia pastoris* strain X-33 was transformed with the empty
171 pPICZalphaB plasmid and with the aldolase constructs and mutant variants
172 cloned in pPICZalphaB using the electroporation protocol described in the Easy
173 Select™ Pichia expression kit manual from Invitrogen (Life Technologies).
174 Methanol induced expression of aldolase variants was carried out in 100 or
175 500mL cultures of the resulting strains as described in this manual using the
176 BMGY and BMMY media described therein. Clarified culture media (Pichia cells
177 removed by centrifugation 1,500 x *g* for 10min at 4°C) was assayed for aldolase
178 enzyme activity, or analysed by SDS-PAGE and western blotting with an anti-
179 aldolase antibody in order to verify presence of the recombinant protein. Un-
180 tagged aldolase was partially purified from media of expressing cultures using
181 $(NH_4)_2SO_4$ fractionation. All of the steps were carried out at 4°C. 35% and 35-
182 65% $(NH_4)_2SO_4$ fractions were desalted using Zeba desalting columns (Thermo-
183 Fischer, product code 89877) as described in the manufacturer's manual and
184 further analysed for aldolase enzyme activity and total protein content. The final
185 buffer for aldolase preparations was [25mM HEPES-NaOH pH 7.0, 2mM $MgCl_2$,
186 1mM EDTA, 0.2mM EGTA, 1mM DTT, 20% (v/v) ethylene glycol] adapted from
187 (Moorhead *et al.*, 1994).
188
189 Arabidopsis total soluble protein was extracted by grinding tissues to a
190 fine powder under liquid N_2 with a pre-chilled (-20°C) mortar and pestle. A

191 volume of extraction buffer [50mM Tris-HCl pH 7.4, 10% (v/v) glycerol, 0.1%
192 (v/v) Triton-X100, 1mM EDTA, 1mM DTT, 1mM phenylmethylsulfonyl-fluoride
193 (PMSF), 5% (w/v) poly-vynil-polypyrrolidone (PVPP)] was added at a ratio of
194 1μLmg^{-1} of tissue. Samples were then centrifuged at 12,000 x *g* for 10min at 4°C.
195 The resulting supernatant represented the total soluble protein crude extract.
196 and further analyzed by enzyme activity assays or by SDS-PAGE and western
197 blotting.
198
199 Enzyme activity was assays were carried out in 1.5mL plastic cuvettes or
200 96-well plates using a Unicam UV/Vis, model UV4, spectrophotometer, or a
201 Beckman-Coulter DTX 880 Multimode Detector plate-reader, respectively.
202 Spectrophotometer assays were in a final volume of 1mL and plate reader assays
203 were carried out in a 200μL volume according to (Graham, 2007). To measure
204 aldolase activity in the presence of polymerised actin, aldolase was added to
205 actin, or BSA-containing samples in low salt buffer (LSB, 5mM Tris-Cl pH8.0,
206 0.2mM $CaCl_2$, 0.2mM ATP, 0.5mM DTT). Polymerisation was induced by addition
207 of 10xPIB (500mM KCl, 20mM $MgCl_2$, 10mM ATP) to a 1x concentration. Samples
208 were allowed to polymerise for 1hr at room temperature and then a mix of
209 Hepes-NaOH pH7.7, NADH, TPI, G3PDH and F1,6BP was added to the same final
210 concentrations as above in a final reaction volume of 200μL. In non-polymerised
211 actin control samples an equivalent volume of LSB was added instead of 10xPIB.
212 For each sample assayed, a control sample without F1,6BP was also measured to
213 control for background NADH absorbance reduction.
214
215 Proteins separated by SDS-PAGE were Coomassie-stained, or transferred
216 to nitrocellulose membranes for western blotting. Ponceau S staining was used
217 to monitor protein transfer and equal sample loading. Aldolase was detected
218 using an anti-cytosolic aldolase, rabbit, primary antibody, described in
219 (Moorhead *et al.*, 1994), and an anti-rabbit antibody conjugated with
220 horseradish peroxidase was used for detection with a WestPico ECL
221 chemiluminescence kit (Thermo-Fischer) following this manufacturer's
222 instructions.
223

224 Co-sedimentation assays with actin were carried out using purified rabbit
225 muscle actin as described in the corresponding datasheet and using the amounts
226 of actin and test proteins (aldolase, or BSA) specified in each experiment in
227 500µL, or 1mL final sample volumes. All proteins were buffer exchanged into
228 LSB prior to use. Centrifugation steps were carried out at 100,000g for 1 hour at
229 25°C.
230
231 For actin polymerisation assays, purified actin suspended in LSB at a
232 concentration of 10mgmL^{-1} was spiked with pyrene-labeled actin (Denver
233 Cytoskeleton Inc.) to 5% (w/w). Reactions were set up in a 200µL final volume
234 containing 8µM pre-cleared actin and aldolase at the molar ratios specified in
235 each experiment. Polymerisation was induced by addition of 10xPIB to a final 1x
236 concentration and monitored by the increase in pyrene-fluorescence.
237 Measurements were made using a Perkin-Elmer 3000 fluorimeter and
238 calculation of the polymerisation half-time and rate at half-time were carried out
239 as described in (Doolittle *et al.*, 2013). Apparent viscosity of actin solutions was
240 measured using falling ball viscometry (Maclean-Fletcher and Pollard, 1980).
241 Each sample was measured in triplicate and two independent samples measured
242 for each aldolase:actin ratio tested.
243
244 Agrobacterium-mediated transient transformation of *Nicotiana tabacum*
245 and *Nicotiana benthamiana* leaves was carried out according to (Sparkes *et al.*,
246 2006). Transformed leaf sections were imaged 48-72hrs after leaf infiltration
247 with Agrobacterium. For transient transformation of *Nicotiana benthamiana,*
248 leaves were co-infiltrated with an Agrobacterium strain containing a P19-
249 expressing binary vector to prevent silencing of the other transiently
250 transformed constructs of interest. Stably transformed Arabidopsis lines were
251 generated using single and double floral-dipping methods described in (Davis *et*
252 *al.*, 2009). The GFP:Lifeact line expressed in the Col-0 background was donated
253 by Professor Patrick Hussey (University of Durham). Seeds of dipped plants were
254 grown on MS-sucrose plates and selected with 15µgmL^{-1} glufosinate ammonium
255 for RFP constructs and 15µgmL^{-1} hygromycin-B for GFP based constructs.

256 Doubly transformed plants were screened with one of the two herbicides and the
257 presence of the additional construct was verified by CLSM.
258
259 Stomatal density measurements were carried out as described in (Jiang *et*
260 *al.*, 2012). Plants were grown in a 'Microclima' growth chamber (Snijders
261 Scientific) with a 22°C/20°C day/night temperature cycle and a 9.5/13.5hrs
262 light/dark cycle separated by two 15min periods of intermediate light intensity
263 and temperature, corresponding to dawn and dusk, for 5-6 weeks. Five-week-old
264 plants were placed on a plastic horticultural tray and viewed under a thermal
265 imaging camera (model SC1000; FLIR Systems, Wilsonville, OR, USA). Thermal
266 images were recorded at 1-min intervals. Leaf temperature was calculated as the
267 average temperature of three different leaves on each of at least three different
268 plants per genotype and plotted over time. For humidity-drop experiments,
269 plants were monitored under daytime growing conditions (see above) for 50min,
270 followed by a pre-programmed drop in the growth chamber's relative humidity
271 from 80% to 40%. The experiments were repeated at least three times
272 independently.
273
274 For growth analysis of Arabidopsis, wild type and mutant plants were
275 germinated and grown for 10-12 days before transfer to soil and growth under
276 normal conditions. Plants were imaged every 2 days, starting 2 days after
277 transplanting and until plants bolted. Images were analysed using LeafLab
278 version 4 software (Professor Mark Fricker, University of Oxford) to calculate
279 total rosette leaf area.
280
281 Confocal laser-scanning microscopy (CLSM) was carried out on a Zeiss
282 (Jena, Germany) Axioplan 2 microscope with a water-dipping, 40x, 1.40NA
283 objective lens, connected to an LSM510 Meta confocal module, or on a Leica
284 (Solms, Germany) TCS-SP5 confocal microscope with a water-dipping, 63x,
285 1.20NA objective lens and appropriate settings for the various fluorophores. For
286 imaging, plant samples were mounted in half-strength MS medium, 1% (w/v)
287 sucrose, 0.05% (w/v) MES pH5.8 with KOH. For imaging guard cells, 4-6 week

old rosette leaves were mounted in 10/50 buffer (10mM KCl, 50mM MES-KOH pH 6.15).

Co-localization analysis and calculation of the various coefficients was carried out using the JaCoP plugin in the Image J software (Bolte and Cordelieres, 2006). The local Pearson's correlation coefficient was estimated on a pixel-by-pixel basis from the structural term of the Structural Similarity Index (SSIM) (Zhou *et al.*, 2004) over an 2-D isotropic Gaussian-weighted region with radius of 5 pixels for each plane of dual-channel 3D (*x,y,z*) images of aldolase-RFP/LifeAct-GFP, free-RFP/LifeAct-GFP, or aldolase-RGP/free-GFP. The resultant map of correlation coefficients was pseudo-colour coded between blue (-1, perfectly inversely-correlated) to red (1, perfectly correlated). For quantitative measurements, values were integrated over an elliptical binary region-of-interest (ROI) manually drawn to select a guard cell pair (excluding the nuclei), and further masked by an automatic intensity threshold from either the aldolase-RFP image or the LifeAct-GFP image to exclude background regions.

FRET-FLIM data was collected using a Leica SP5 confocal microscope connected to a PicoQuant (Berlin, Germany) PicoHarp 300, TCSPC (time-correlated single photon counting) FLIM module. FLIM images of GFP:Lifeact were acquired using a 470nm, pulsed laser for excitation and detector set to collect fluorescence between 500-560nm. 256x256 pixel images were collected until 1000 counts were achieved for each pixel. Post-acquisition analysis was carried out using the SymPhoTime 64 software from PicoQuant. The lifetimes of all the images per fluorophore combination were averaged and compared for the guard cells excluding the auto-fluorescence for the pore lips.

Results:

Plant aldolase interacts with actin *in vitro*

To determine whether plant aldolase interacts with actin and the impact on the functional properties of the two proteins, *in vitro* tests were conducted with purified recombinant AtFBA8 and actin. AtFBA8 co-sedimented with

319 polymerised F-actin, but not G-actin, in a concentration dependent manner.
320 Thus, using SDS-PAGE and Coomassie blue staining, aldolase was detected in the
321 supernatant fractions of G-actin and aldolase-only co-sedimentation samples, but
322 the majority of aldolase was detected in the pellet fraction of the F-actin sample,
323 with only traces being detectable in the corresponding supernatant (Fig. 1A,
324 dashed arrow). In a similar co-sedimentation experiment increasing amounts of
325 aldolase were added to a fixed amount of actin (Fig. 1B) and aldolase was
326 quantified by immuno-detection. At aldolase to actin monomer molar ratios of
327 0.3 or lower the majority of aldolase was associated with actin. Whereas, at
328 molar ratios of 0.6 and above, the amount of aldolase co-pelleting with actin
329 appeared to be saturated and additional aldolase accumulated in the
330 supernatant.
331
332 The effects of aldolase binding on actin bundling and polymerisation were
333 also investigated. Addition of aldolase at a molar ratio of 0.1 to F-actin led to a
334 significant increase in viscosity compared to F-actin alone when measured by
335 falling-ball viscometry (Fig. 2A). Further addition of aldolase at higher molar
336 ratios to actin decreased viscosity to levels comparable to that of F-actin alone,
337 as has been reported for other actin bundling proteins (Wang *et al.*, 1996).
338 However, addition of aldolase had no effect on actin polymerisation kinetics in
339 pyrene fluorescence assays (Supplementary Fig. S1 and S2).
340
341 Reciprocally, aldolase enzyme activity assays showed that aldolase
342 activity was significantly inhibited (3-fold decrease) in the presence of F-actin,
343 but not G-actin or equimolar amounts of BSA. This was the case at both 5μM
344 fructose 1,6-bisphosphate (F1,6-BP), which is close to the previously reported
345 plant cytosolic aldolase K_M of 6μM (Moorhead and Plaxton, 1990), and at a
346 saturating concentration of 5mM F1,6-BP (Fig. 2B). Aldolase activity was further
347 measured in the presence of increasing amounts of F-actin (0-100μgmL^{-1}),
348 corresponding to a decrease in the aldolase to actin molar ratio from 1.4 to 0.07)
349 at a range of F1,6-BP concentrations (0-60μM). Michaelis-Menten curves were
350 fitted to the resulting data (Fig. 2C) and the kinetic parameters of aldolase at
351 each concentration of F-actin were calculated from these curves (Table 1). The

352 inhibitory effect of actin was concentration dependent. At F-actin concentrations
353 of 0-10μgmL^{-1} (molar ratio of aldolase to actin: infinity-0.7) there was a slight
354 but progressive decrease in the aldolase V_{max} with the K_M remaining stable.
355 Aldolase activity further decreased by two orders of magnitude and then became
356 undetectable at 50 and 100μgmL^{-1} F-actin (molar ratios of 0.14 and 0.07),
357 respectively (Fig. 2C and Table 1). We infer from these data that plant aldolase
358 can interact with F-actin *in vitro*, and the binding interaction has the potential to
359 affect both the enzymatic activity of aldolase and the structure of the F-actin
360 network.
361

362 **Assessing association of aldolase with F-actin *in vivo.***

363 To determine whether aldolase FBA8 interacts with actin *in vivo*, we first
364 sought to construct a fluorescently-tagged version of FBA8 that would
365 functionally complement an FBA8-knockout Arabidopsis line (*fba8-1*). The *FBA8*
366 coding sequence driven by the Arabidopsis ubiquitin-10 promoter was fused C-
367 terminally with that of red fluorescent protein RFP (mRFP1). Expression of the
368 full-length fusion protein was verified by western blot with an anti-aldolase
369 antibody (Fig. 3A, solid arrow). Native aldolase was detectable in the wild type
370 control at 40kD molecular weight, but not in the *fba8-1* genetic background of
371 the transformants (Fig. 3A, dashed arrow). Intact aldolase:RFP in the
372 complemented lines appeared at the expected 70kD (Fig. 3A, solid arrow), along
373 with a cleavage product of the expected Mw of native aldolase. We assume that
374 the partner cleavage product yielding free RFP might also be present in these
375 lines, although we have not tested for its presence directly. Overall, FBA8-RFP
376 protein level in the complemented lines was similar to wild type aldolase
377 abundance. The complemented lines restored normal levels of germination and
378 growth to the *fba8-1* mutant (Supplementary Fig. S3 and S4).
379

380 The subcellular localization of aldolase:RFP was compared to that of free
381 RFP *in planta* using confocal laser-scanning microscopy (CLSM). Both
382 aldolase:RFP and free RFP localized to the cytosol and the majority of
383 fluorescence was homogeneously distributed, with smaller organelles (such as

384 mitochondria) appearing in negative contrast. Free RFP (Mr 30kD) was able to
385 enter the nucleus, whilst aldolase:RFP (Mr 70kD) was excluded as expected from
386 the molecular weight cutoff size for protein import into the nucleus. Other than
387 this, no major difference in the distribution of the two fluorescent proteins was
388 evident in root epidermal (Fig. 3B), hypocotyl cells (Fig. 3C), and in most other
389 cell types studied, including: root meristem, root vascular and leaf epidermal
390 cells (data not shown). However, in stomatal guard cells and to a lesser extent in
391 leaf epidermal cells, a small proportion of aldolase:RFP was observed in
392 association with fine filaments (Fig. 4A). In these cell types, aldolase:RFP was
393 again excluded from chloroplasts and nuclei, but some signal was detectable in
394 vacuoles that might reflect degradation of the aldolase:RFP observed in the
395 Western blots (Fig. 3A).
396
397 To test whether filamentous structures formed by aldolase:RFP represent
398 instances of aldolase associating with actin, complemented *fba8-1* plants
399 expressing aldolase:RFP, or Col-0 plants expressingfree RFP (as a control for a
400 cytosolic protein not expected to associate with actin), were co-transformed with
401 GFP:Lifeact, which binds to actin filaments (Riedl *et al.*, 2008). As an additional
402 control for cytosolic protein colocalisation, complemented *fba8-1* plants
403 expressing aldolase:RFP were also co-transformed with free cytosolic GFP. As
404 expected, GFP:Lifeact labeled bundles and filaments of various thickness
405 throughout the cytoplasm of guard cells and leaf epidermal cells (Fig. 4A and B),
406 whilst free GFP was found throughout the cytosol, including cytoplasmic strands
407 across the vacuole, and also within the nuclei (Fig. 4C). Merged images
408 suggested some degree of co-localization between aldolase:RFP and GFP:Lifeact
409 (Fig. 4A), but the degree of overlap was comparable to that seen in free
410 RFP/GFP-lifeact images (Fig. 4B). Quantitative measurements of co-localisation
411 using a suite of metrics including Pearson's correlation coefficient (PCC) and
412 Manders overlap coefficients indicated some degree of co-localisation between
413 aldolase:RFP and GFP:lifeact, but it was not significantly higher than that
414 observed for free RFP and GFP:lifeact (Table 2). Conversely, there was a very
415 high degree of visual overlap and correlation coefficient between free GFP and
416 aldolase-RFP, except for the nuclei, where the latter is excluded. Van Steensel's

417 cross correlation functions, Li's intensity correlation analysis, and Coste's
418 analysis (Bolte and Cordelieres, 2006) were also carried out on the same images
419 and also revealed no differences between aldolase:RPF and free RFP association
420 with GFP:Lifeact (Supplementary Table S2). Given that these correlation metrics
421 are averaged over the entire image, we further investigated spatially localized
422 estimates of PCC calculated as part of a Structural Similarity Index (SSIM)
423 measure (Zhou *et al.* 2004). However, pseudo-colour coded maps of the PCC
424 calculated for circular, Gaussian weighted regions around each pixel did not
425 provide evidence for higher co-localisation of aldolase:RFP along GFP:Lifeact
426 filaments (Fig. 4A-C). Taken together, we were not able to find quantitative
427 evidence for *in vivo* interaction between aldolase and actin using co-localisation
428 analysis. This finding is perhaps not surprising considering that only a small
429 fraction of total cellular aldolase may be bound to actin against a much more
430 substantial background of unbound, cytosolic aldolase, and confocal imaging
431 does not have sufficient spatial resolution to discriminate bound from free
432 aldolase.
433
434 We therefore sought a more specific test of interaction between
435 aldolase:RFP and GFP:Lifeact *in vivo* using fluorescence resonance energy
436 transfer-fluorescence lifetime imaging microscopy (FRET-FLIM). Measuring the
437 change of lifetime, if any, in GFP:Lifeact-aldolase:RFP co-expressing cells has the
438 benefit of eliminating any background signal from unbound cytosolic
439 aldolase:RFP (or cleaved free RFP), since the GFP:Lifeact fluorescence lifetime is
440 only sensitive to actin-bound aldolase:RFP within a few nm. Representative GFP
441 lifetime images of Arabidopsis guard cells expressing GFP:Lifeact alone and co-
442 expressing aldolase:RFP are shown in Fig. 5A. The majority of the cytoplasmic
443 GFP:Lifeact signal was within 2.3-2.7 ns, whilst the autofluorescence from the
444 pore lip showed a much longer lifetime of around 10 ns (Fig. 5A). However, the
445 average lifetime fit to the exponential decay curves showed evidence for an
446 interaction between aldolase:RFP and GFP:Lifeact as a slight, but significant,
447 decrease in the average lifetime. Thus, the average lifetime of GFP:Lifeact alone
448 was around 2.43ns but decreased to 2.39 ns when co-expressed with
449 aldolase:RFP (Fig. 5B). Similar results were found in transiently transformed

450 tobacco leaf epidermal cells (Fig. 5C). GFP:Lifeact alone or when it was co-
451 expressed with free RFP had an average lifetime of 2.60ns and 2.55ns,
452 respectively. When co-expressed with aldolase:RFP it had a significantly lower
453 average lifetime of 2.43ns.
454
455 If aldolase does indeed interact *in vivo* with actin at low concentration, we
456 would predict from the *in vitro* data that it might serve to stabilize or bundle
457 actin filaments. We therefore examined whether loss of aldolase in the *fba8-1*
458 mutant perturbed actin cytoskeleton organisation. The structure of actin was
459 compared by CLSM in guard cells of *fba8-1* and wild type plants expressing the
460 actin-binding GFP:Lifeact to visualise actin filaments and cables *in vivo*. There
461 was no major difference in the structure of the actin network between the two
462 lines. However, GFP:Lifeact in the *fba8-1* line (Fig. 6A) was slightly more diffuse,
463 with fewer thick actin cables compared to wild type or aldolase:RFP
464 complemented cells (Fig. 6B and C).
465

466 **Assessing the importance of aldolase FBA8 for guard cell function.**

467 As the cellular phenotype of the *fba8-1* mutant is quite subtle and
468 challenging to quantify, we sought to assess the importance of aldolase FBA8 for
469 guard cell function by characterizing physiological responses in the *fba8-1*
470 aldolase knockout line (Fig. 7A and B). This line had greatly decreased cytosolic
471 aldolase protein levels as verified by western blot with an anti-cytosolic aldolase
472 antibody (Fig. 7C) and significantly decreased aldolase enzyme activity in roots
473 (Fig. 7D) as measured by aldolase activity assays in crude protein extracts. It also
474 displayed moderately slow growth phenotypes, with *fba8-1* seedlings
475 germinated on MS agar plates without sucrose being smaller than wild type Col-
476 0 at one week old (Supplementary Fig. S3A). Additionally, rosettes of *fba8-1*
477 plants grown on sucrose supplemented MS agar plates and then transferred to
478 soil at two weeks old were smaller by 3 weeks old (Supplementary Fig. S3B and
479 C). This apparent difference in size was further confirmed by measuring rosette
480 leaf area of 24 individual plants per genotype (Supplementary Fig. S3D).
481

482 To assess guard cell function in the *fba8-1* and complemented
483 aldolase:RFP lines we used thermal imaging measurements of leaf temperature
484 as a proxy for transpiration over 24h day-night cycles. No differences in
485 response were observed during dawn or dusk transitions (low light with
486 increasing or decreasing temperature, respectively), or day (high light, 22°C) or
487 night (dark, 20°C) conditions (Supplementary Fig. S5). However, during
488 transition from high (80%) to low (40%) relative humidity (RH) the leaf
489 temperature of *fba8-1* rosettes dropped to a greater extent than that of wild type
490 or the complemented aldolase:RFP lines indicating greater stomatal aperture
491 than wild type (Fig. 8). Thus, all three genotypes had similar temperatures under
492 normal humidity conditions (Fig. 8, note overlapping traces in the left portion of
493 the graph). However, upon reduction of humidity (dashed line) *fba8-1* leaves
494 dropped to around 0.5°C cooler than those of Col-0 and aldolase:RFP over an
495 extended period implying that *fba8-1* stomata reached a different set point in
496 response to a change in RH. Moreover, this result was not caused by a difference
497 in the density of stomata in *fba8-1* leaves (Supplementary Fig. S6).

498 **Discussion**

499

500 The data we have presented demonstrate that Arabidopsis aldolase FBA8
501 is capable of binding F-actin *in vitro* in a similar manner to aldolase from other
502 organisms (Arnold and Pette, 1970; Wang *et al.*, 1996; Holtgrawe *et al.*, 2005).
503 Moreover, this interaction affected the function of both these proteins. The effect
504 of aldolase on F-actin viscosity we observed is most likely related to the presence
505 of two putative actin-binding domains (Forlemu *et al.*, 2007) in the tetrameric
506 aldolase holoenzyme (Moorhead and Plaxton, 1990) enabling it to bind two actin
507 filaments simultaneously (Supplementary Fig. S7) and thereby act as an actin
508 bundling protein. Indeed, addition of recombinant FBA8 to F-actin solutions and
509 measurement of the concurrent change in viscosity generated a profile almost
510 identical to that previously reported for rabbit muscle aldolase (Wang *et al.*,
511 1996) and similar to that expected for actin bundling proteins in general
512 (Gungabissoon *et al.*, 2001). Wojtera-Kwiczor et al. (2012) previously proposed
513 that FBA6, a different cytosolic isoform of Arabidopsis aldolase, bundled actin

514 under oxidizing but not under reducing conditions based on their results of actin
515 phaloidin-staining followed by CLSM imaging. It was suggested that such
516 bundling of actin by aldolase under oxidising conditions may be part of a greater
517 signaling cascade occurring in response to changes in cellular redox conditions.
518 Thus, aldolase may have a secondary role as an actin bundling protein.
519
520 In addition, we have shown that binding of aldolase to actin has reciprocal
521 effects on aldolase enzyme activity, resulting in non-competitive inhibition by F-
522 actin but not by equal amounts of G-actin or BSA. This effect is most likely due to
523 steric hindrance of the active site cleft upon binding actin filaments. To
524 understand whether these quite strong reciprocal interactions observed *in vitro*
525 have any significance *in vivo* we sought to demonstrate first that aldolase
526 interacts with actin *in vivo*; second, whether this interaction affects actin
527 organization; and third, whether there is an effect on guard cell physiology as a
528 consequence. However, as any aldolase-actin interaction takes place against a
529 much greater background of free cytoplasmic aldolase and is well below the
530 resolution of CLSM it was not possible to identify co-localisation of a small
531 fraction of the aldolase pool with actin using conventional co-localisation
532 analysis, even when using local correlation measures. Nevertheless, our data
533 provide some support for microcompartmentation of aldolase FBA8 in guard
534 cells using FRET-FLIM measurements of GFP:Lifeact when co-expressed either
535 with aldolase:RFP as a much more specific measure of protein proximity, in
536 either Arabidopsis guard cells or tobacco leaf epidermal cells. Our results show
537 that in both cell types GFP:Lifeact has a significantly shorter lifetime when co-
538 expressed with aldolase:RFP than GFP:Lifeact on its own or when co-expressed
539 with free RFP. This finding suggests strongly that aldolase:RFP remains in
540 proximity with GFP:Lifeact long enough to cause a reduction in the latter's
541 fluorescence emission life-time. The simplest explanation for this observed effect
542 is that the two fluorophores are anchored within a FRET-compatible distance
543 (<10nm) by associating with actin filaments. The shift in lifetime is still small,
544 possibly because we would still only expect a small number of aldolase-RFP
545 molecules to bind within the Förster radius of the GFP-Lifeact molecules in an
546 appropriate configuration for FRET.

547

548 Given the *in vitro* actin bundling property of aldolase FBA8, a potential
549 role for the enzyme in guard cells could be to modify the actin cytoskeleton and
550 thus modulate guard cell behaviour. Extensive reorganisation of the guard cell
551 actin network occurs during stomatal movements (Kim *et al.*, 1995; Jiang *et al.*,
552 2012), and actin re-organisation is a critical link in model of ABA-induced guard
553 cell behavior (Li *et al.*, 2006). Previous work suggested that the polymeric state
554 of actin affects guard cell motions, ostensibly by modulating inward rectifying
555 K^+-channel activity. Cytochalasin-D treatments (which induce actin
556 depolymerisation) of *Vicia faba* and *Commelina communis* leaves enhanced light-
557 induced stomatal opening, while actin filament stabilizing agents inhibit this
558 process (Kim *et al.*, 1995; Hwang *et al.*, 1997). We observed an effect of aldolase
559 on actin bundling *in vitro* (Fig. 2) rather than actin polymerisation kinetics
560 directly (Supplementary Fig. S1 and S2), but we infer that this might alter the
561 organization of the actin network, and visual assessment of the actin filament
562 network in *fba8-1* knockout guard cells suggested a subtle decrease in actin cable
563 thickness in *fba8-1* stomata and with a more random orientation compared to
564 the thicker radial distribution of actin cables in wild type guard cells (Fig. 6). This
565 subtle cellular phenotype was matched by a subtle change in physiological
566 responses: stomatal function in *fba8-1* leaves was unaffected under normal
567 growth conditions (Supplementary Fig. S5). However, we showed that the *fba8-1*
568 knockout line has altered stomatal responses to humidity changes: in the
569 absence of FBA8, stomatal closure in response to low humidity was slightly
570 impaired impaired (Fig. 8). This suggests that aldolase FBA8 is requisite at least
571 for some aspects of guard cell motion.

572

573 It is not possible to discern from our data whether this change in guard
574 cell function is related to the metabolic function of aldolase or to a secondary
575 role as an actin bundling protein. Indeed, a metabolic effect is plausible, given
576 previous studies on knockout Arabidopsis lines of the glycolytic enzyme
577 phosphoglycerate mutase showed a similarly slow response to ABA-induced
578 closure (Zhao and Assmann, 2011). Since stomatal response to low humidity is
579 primarily ABA-mediated (Assmann *et al.*, 2000; Xie *et al.*, 2006; Bauer *et al.*,

580 2013), it is conceivable that the delay in stomatal closure we observed is caused
581 by a general metabolic impairment in glycolytic enzyme-knockout stomata and
582 not related to aldolase microcompartmentation directly. Aldolase is required for
583 both glycolysis and gluconeogenesis. While glycolysis (and thus aldolase) is
584 clearly implicated in supplying carbon for malate production during stomatal
585 opening (Vavasseur and Raghavendra, 2005), roles for glycolysis and/or
586 gluconeogenesis during stomatal closure are less obvious. Results of ^{14}C-malate
587 feeding experiments suggest that malate, exported from the vacuole during
588 stomatal closure, is decarboxylated and converted to starch via gluconeogenesis
589 (Outlaw, 1982). It was suggested that this is the main metabolic fate of malate
590 during stomatal closure (Schroeder *et al.*, 2001). However, it has also been
591 argued that the rate of malate conversion to starch in closing stomata is 3 orders
592 of magnitude slower than stomatal closure itself, and that key enzymes activities
593 necessary for malate-fueled gluconeogenesis (such as pyruvate-phosphate
594 dikinase and posph*oenol*pyruvate carboxykinase) are absent or very low in
595 guard cells. Thus malate export from guard cells was proposed as an alternative
596 (Outlaw, 2003). Our data from the *fba8-1* line and prior results from
597 phosphoglycerate mutase knockout lines (Zhao and Assmann, 2011) are both
598 consistent with a role for glycolysis or gluconeogenesis during ABA-mediated
599 stomatal closure.
600
601 Ultimately, to discriminate between the enzymatic and actin-binding roles
602 of aldolase, it will be necessary to genetically uncouple these two activities *in*
603 *vivo*. We made concerted attempts to do this by mutating residues in aldolase
604 that are thought to be responsible for actin binding (Supplementary Fig. S7).
605 Unfortunately, the rather large change in charge caused by replacement of
606 multiple residues affected the stability or folding of the protein, as we were
607 unable to successfully express this mutant aldolase in Arabidopsis, yeast, or *E.*
608 *coli* (data not shown).
609
610 In summary, we show clearly that plant aldolase can be
611 microcompartmented *in vitro* as observed previously for mammalian aldolase,
612 but identifying the extent that this occurs *in vivo* and the significance has proved

613 to be more challenging. Our experiments provide some evidence that suggest
614 this interaction also takes place *in vivo* and has some relevance. Firstly,
615 aldolase:RFP but not free RFP formed filamentous structures, in addition to the
616 expected homogeneous cytoplasmic distribution, that were reminiscent of the
617 cytoskeleton. These filamentous structures co-localized with GFP:lifeact and
618 resulted in a small, but significant decrease in the lifetime of GFP:lifeact in FRET-
619 FLIM experiments. This last line of evidence is crucial, as it demonstrates a clear
620 difference in the behavior of aldolase:RFP compared to free RFP, which is a
621 presumably 'unbound' cytosolic protein. The consequence of normal FBA8
622 binding was assessed in *fba8-1* mutant lines that showed both a subtle decrease
623 in actin network structure and a reduced closing response to a humidity drop.
624 Thus we provide preliminary evidence for possible roles of aldolase in
625 organization of the actin cytoskeleton in stomatal guard cells, thereby
626 complementing previous findings, which suggest that Arabidopsis cytosolic
627 aldolases moonlight as actin bundling proteins.

628 **Supplementary Data**

629 Supplementary Table S1: Primers and PCR annealing temperatures used;
630 Supplementary Table S2: Metrics of aldolase:RFP and free RFP co-localisation
631 with GFP:Lifeact in Arabidopsis guard cells;
632 Supplementary Figure S1: Pyrene fluorescence assay of actin polymerisation in
633 the presence of recombinant aldolase;
634 Supplementary Figure S2: Kinetics of actin polymerisation in the presence of
635 recombinant aldolase;
636 Supplementary Fig. S3: Germination and growth phenotypes of *fba8-1* aldolase-
637 knockout line;
638 Supplementary Fig. S4: Complementation of *fba8-1* phenotypes by aldolase:RFP;
639 Supplementary Fig. S5: Thermal imaging data on *fba8-1* during a normal growth
640 cycle;
641 Supplementary Fig. S6: Stomatal density and index of the *fba8-1* line;
642 Supplementary Fig. S7: Identification of putative actin-binding residues and sites
643 of Arabidopsis FBA8;

Acknowledgements:

CG would like to thank Doctors: B. Ghel, A. Kugler, M. Laxa, N. Irani, M. Kalde and B. O'Leary (University of Oxford, UK) for their invaluable help and training in experimental techniques during this project. We thank Dr. M. Schwarzlander (University of Bonn, Germany) for the roGFP2 expression vector, Professor B. Davis and B. Bhushan (University of Oxford, UK) for help with expressing recombinant aldolase and Professor W. Plaxton (Queen's University, Ontario, Canada) for the anti-aldolase antibody. We also thank Dr. Ian Moore (University of Oxford, UK) for help and advice with CLSM experimental design.

CG and LJS acknowledge funding from the Gatsby Charitable foundation.

Declaration of Interest: The authors declare no conflicts of interest.

Contribution Statement: CG conducted experiments and wrote the paper; MDF conducted experiments, provided analytical software, and wrote the paper; KIK, TJH, and IC provided technical expertise, and helped design and conduct experiments; PJH and AMH helped design experiments and contributed materials for their completion; LJS conceived and designed experiments, and wrote the paper.

References:

An S, Deng YJ, Tomsho JW, Kyoung M, Benkovic SJ. 2010. Microtubule-assisted mechanism for functional metabolic macromolecular complex formation. *Proceedings of the National Academy of Sciences of the United States of America* **107**, 12872-12876.

An S, Kumar R, Sheets ED, Benkovic SJ. 2008. Reversible compartmentalization of de novo purine biosynthetic complexes in living cells. *Science* **320**, 103-106.

Arnold H, Pette D. 1970. Binding of aldolase and triosephosphate dehydrogenase to F-actin and modification of catalytic properties of aldolase. *European Journal of Biochemistry* **15**, 360-366.

Assmann SM, Snyder JA, Lee Y-rJ. 2000. ABA-deficient (*aba1*) and ABA-insensitive (*abi1-1, abi2-1*) mutants of Arabidopsis have a wild-type stomatal response to humidity. *Plant Cell and Environment* **23**, 387-395.

Atteia A, Adrait A, Brugiere S, Tardif M, van Lis R, Deusch O, Dagan T, Kuhn L, Gontero B, Martin W, Garin J, Joyard J, Rolland N. 2009. A proteomic survey of Chlamydomonas reinhardtii mitochondria sheds new light on the metabolic plasticity of the organelle and on the nature of the alpha-proteobacterial mitochondrial ancestor. *Molecular Biology and Evolution* **26**, 1533-1548.

Balasubramanian R, Karve A, Kandasamy M, Meagher RB, Moore BD. 2007. A role for F-Actin in hexokinase-mediated glucose signaling(1[C][W][OA]). *Plant Physiology* **145**, 1423-1434.

Barkla BJ, Vera-Estrella R, Hernandez-Coronado M, Pantoja O. 2009. Quantitative proteomics of the tonoplast reveals a role for glycolytic enzymes in salt tolerance. *The Plant Cell* **21**, 4044-4058.

Bauer H, Ache P, Lautner S, Fromm J, Hartung W, Al-Rasheid KA, Sonnewald S, Sonnewald U, Kneitz S, Lachmann N, Mendel RR, Bittner F, Hetherington AM, Hedrich R. 2013. The stomatal response to reduced relative humidity requires guard cell-autonomous ABA synthesis. *Current biology : CB* **23**, 53-57.

Bolte S, Cordelieres FP. 2006. A guided tour into subcellular colocalization analysis in light microscopy. *Journal of Microscopy-Oxford* **224**, 213-232.

Chuong SD, Good AG, Taylor GJ, Freeman MC, Moorhead GB, Muench DG. 2004. Large-scale identification of tubulin-binding proteins provides insight on subcellular trafficking, metabolic channeling, and signaling in plant cells. *Molecular Cell Proteomics* **3**, 970-983.

Davis AM, Hall A, Millar AJ, Darrah C, Davis SJ. 2009. Protocol: Streamlined sub-protocols for floral-dip transformation and selection of transformants in *Arabidopsis thaliana*. *Plant Methods* **5**.

Deeks MJ, Fendrych M, Smertenko A, Bell KS, Oparka K, Cvrckova F, Zarsky V, Hussey PJ. 2010. The plant formin AtFH4 interacts with both actin and microtubules, and contains a newly identified microtubule-binding domain. *Journal of Cell Science* **123**, 1209-1215.

Doolittle LK, Rosen MK, Padrick SB. 2013. Measurement and analysis of *in vitro* actin polymerization. *Methods in Molecular Biology* **1046**, 273-293.

Feric M, Vaidya N, Harmon TS, Mitrea DM, Zhu L, Richardson TM, Kriwacki RW, Pappu RV, Brangwynne CP. 2016. Coexisting liquid phases underlie nucleolar subcompartments. *Cell* **165**, 1686-1697.

Forlemu NY, Waingeh VF, Ouporov IV, Lowe SL, Thomasson KA. 2007. Theoretical study of interactions between muscle aldolase and F-actin: Insight into different species. *Biopolymers* **85**, 60-71.

Giege P, Heazelwood, Roessner-Tunali, Millar H, Fernie AR, Leaver CJ, Sweetlove LJ. 2003. Enzymes of glycolysis are functionally associated with the mitochondrion in Arabidopsis cells. *The Plant Cell* **15**, 2140-2151.

Gierasch LM, Gershenson A. 2009. Post-reductionist protein science, or putting Humpty Dumpty back together again. *Nature Chemical Biology* **5**, 774-777.

Graham JW, Williams TC, Morgan M, Fernie AR, Ratcliffe RG, Sweetlove LJ. 2007. Glycolytic enzymes associate dynamically with mitochondria in response to respiratory demand and support substrate channeling. *The Plant Cell* **19**, 3723-3738.

Graham JWA. 2007. Mitochondrial glycolysis in plants. *DPhil Thesis, University of Oxford*.

Grefen C, Donald N, Hashimoto K, Kudla J, Schumacher K, Blatt M, R. 2010. A ubiqutin-10 promoter-based vector set for fluorescent tagging facilitates temporal stability and native distrbution in transient and stable expression studies. *The Plant Journal* **64**, 355-365.

Guex N, Peitisch MC. 1997. SWISS-MODEL and the Swiss-PdbViewer: An environment for comparative protein modeling. *Electrophoresis* **18**, 2714-2723.

Gungabissoon RA, Khan S, Hussey PJ, Maciver SK. 2001. Interaction of elongation factor 1α from *Zea mays* (ZmEF-1α) with F-actin and interplay with the maize actin severing protein, ZmADF3. *Cell Motility and the Cytoskeleton* **49**, 104-111.

Holtgrawe D, Scholz A, Altmann B, Scheibe R. 2005. Cytoskeleton-associated, carbohydrate-metabolizing enzymes in maize identified by yeast two-hybrid screening. *Physiologia Plantarum* **125**, 141-156.

Hrazdina G, Wagner GJ. 1985. Metabolic pathways as enzyme complexes: Evidence for the synthesis of phenylpropanoids and flavonoids on membrane associated enzyme complexes. *Archives of Biochemistry and Biophysics* **237**, 88-100.

Hruz T, Laule O, Szabo G, Wessendorp F, Bleuler S, Oertle L, Widmayer P, Gruissem W, Zimmermann P. 2008. Genevestigator v3: a reference expression database for the meta-analysis of transcriptomes. *Advances in Bioinformatics* **2008**, 420747.

Huang S, Taylor NL, Narsai R, Eubel H, Whelan J, Millar AH. 2009. Experimental analysis of the rice mitochondrial proteome, its biogenesis, and heterogeneity. *Plant Physiology* **149**, 719-734.

Hudder A, Nathanson L, Deutscher MP. 2003. Organization of Mammalian Cytoplasm. *Molecular and Cellular Biology* **23**, 9318-9326.

Hwang J-U, Suh S, Yi H, Kim J, Lee Y. 1997. Actin filaments modulate both stomatal opening and inward rectifying K+-channel activities in guard cells of *Vicia faba* L. *Plant Physiology* **115**, 335-342.

Jiang K, Sorefan K, Deeks MJ, Bevan M, Hussey PJ, Hetherington AM. 2012. The ARP2/3 complex mediates guard cell actin reorganization and stomatal movement in Arabidopsis. *The Plant Cell* **24**, 2031-2040.

Kim M, Hepler PK, Eun S-O, Ha KS, Lee Y. 1995. Actin filaments in mature guard cells are radially distributed and involved in stomatal movement. *Plant Physiology* **109**, 1077-1084.

Li S, Assmann SM, Albert R. 2006. Predicting essential components of signal transduction networks: A dynamic model of guard cell absicic acid signaling. *PLoS Biology* **4**, 1732-1748.

Maclean-Fletcher SD, Pollard TD. 1980. Viscometric analysis of the gelation of Acanthamoeba extracts and purification of 2 gelation factors. *Journal of Cell Biology* **85**, 414-428.

Moller BL. 2010. Dynamic Metabolons. *Science* **330**, 1328-1329.

Moorhead G, BG., Hodgson RJ, Plaxton WC. 1994. Copurification of cytosolic fructose 1,6-bisphosphatase and cytosolic aldolase from endosperm of germinating castor oil seeds. *Archives of Biochemistry and Biophysics* **312**, 326-335.

Moorhead G, BG., Plaxton WC. 1990. Purification and characterization of cytosolic aldoalse from carrot storage root. *Biochemical Journal* **269**, 133-139.

Olah J, Norris V, Ovadi J. 2015. Modeling of sensing potency of cytoskeletal systems decorated with metabolic enzymes. *Journal of Theoretical Biology* **365**, 190-196.

Outlaw WHJ. 1982. *Carbon metabolism in guard cells*. New York: Springer Science.

Outlaw WHJ. 2003. Integration of cellular and physiological functions of guard cells. *Critical Reviews in Plant Sciences* **22**, 503-529.

Riedl J, Crevenna AH, Kessenbrock K, Yu JH, Neukirchen D, Bista M, Bradke F, Jenne D, Holak TA, Werb Z, Sixt M, Wedlich-Soldner R. 2008. Lifeact: a versatile marker to visualize F-actin. *Nature Methods* **5**, 605-607.

Sayle R, Milner-White JE. 1995. RasMol: Biomolecular graphics for all. *Trends in Biochemical Sciences* **20**.

Schroeder JI, Allen GJ, Hugouvieux V, Kwak JM, Waner D. 2001. Guard cell signal transduction. *Annual Reviews in Plant Physiology and Plant Molecular Biology* **52**, 627-658.

Schwarzlander M, Fricker MD, Sweetlove LJ. 2009. Monitoring the in vivo redox state of plant mitochondria: effect of respiratory inhibitors, abiotic stress and assessment of recovery from oxidative challenge. *Biochimica Et Biophysica Acta* **1787**, 468-475.

Sparkes IA, Runions J, Kearns A, Hawes C. 2006. Rapid, transient expression of fluorescent fusion proteins in tobacco plants and generation of stably transformed plants. *Nature Protocols* **1**, 2019-2025.

Sullivan DTMR, Fuda N., Fiori J., Barilla J., Ramirez L. 2003. Analysis of glycolytic enzyme co-localization in Drosophila flight muscle. *The Journal of Experimental Biology* **206**, 2031-2038.

Sweetlove LJ, Fernie AR. 2013. The spatial organization of metabolism within the plant cell. *Annual Review of Plant Biology* **64**, 723-746.

Vavasseur A, Raghavendra AS. 2005. Guard cell metbolism and CO2 sensing. *New Phytologist* **165**, 665-682.

Wang J, Morris AJ, Tolan DR, Pagliaro Len. 1996. Molecular nature of the F-actin binding activity of aldolase revealed with site-directed mutants. *The Journal of Biological Chemistry* **271**, 6861-6865.

Wojtas K, Slepecky N, von Kalm L, Sullivan DT. 1997. Flight muscle function in *Drosophila* requires colocalization of glycolytic enzymes. *Molecular Biology of the Cell* **8**, 1665-1675.

Wojtera-Kwiczor J, Gross F, Leffers HM, Kang M, Schneider M, Scheibe R. 2012. Transfer of a redox-signal through the cytosol by redox-dependent microcompartmentation of glycolytic enzymes at mitochondria and actin cytoskeleton. *Frontiers in Plant Science* **3**, 284.

Xie X, Wang Y, Williamson L, Holroyd GH, Tagliavia C, Murchie E, Theobald J, Knight MR, Davies WJ, Leyser HM, Hetherington AM. 2006. The identification of

genes involved in the stomatal response to reduced atmospheric relative humidity. *Current Biology : CB* **16**, 882-887.

Zhao Z, Assmann SM. 2011. The glycolytic enzyme, phosphoglycerate mutase, has critical roles in stomatal movement, vegetative growth, and pollen production in Arabidopsis thaliana. *Journal of Experimental Botany* **62**, 5179-5189.

Zhou W, Bovik AC, Sheikh HR, Simoncelli EP. 2004. Image quality assessment: from error visibility to structural similarity. *IEEE Transactions on Image Processing* **13**, 600-612.

Tables, Figure legends, Figures

Table 1: Kinetic parameters of recombinant aldolase FBA8 in the presence of F-actin

	[Actin] µgmL^{-1} (aldolase to actin monomer molar ratio)				
Aldolase kinetic parameter	**0 (*)**	**5 (1.4)**	**10 (0.7)**	**50 (0.14)**	**100 (0.07)**
K_M for F1,6-BP (µM)	3.6	5.4	5.4	*	*
V_{max} (U mg^{-1})	0.054	0.046	0.042	0.001	0

(* not applicable)

Table 2: Co-localisation parameters of aldolase:RFP with GFP:Lifeact or free GFP, and of free RFP with GFP:Lifeact

Co-localisation coefficient*:	GFP:Lifeact/ aldolase:RFP	GFP:Lifeact / free RFP	Free GFP/ Aldolase:RFP
Pearson's	0.50±0.01	0.52±0.02	0.73±0.01
Overlap	0.80±0.01	0.80±0.02	0.85±0.01
Manders M1 (GFP:Lifeact)	0.47±0.05	0.57±0.06	0.81±0.07
Manders M2 (aldolase:RFP/free RFP)	0.38±0.03	0.42±0.05	0.69±0.04

* Values are the average of each co-efficient ± S.E.M. calculated from a minimum of six independent CLSM, z-stack image series (n=6), for each of the individual co-expressing lines.

** **Figure 1: Association of aldolase with actin *in vitro*.** A) An actin co-sedimentation assay using recombinant Arabidopsis aldolase. Reagents added to each sample are shown in the table above the gel image. Samples were allowed to polymerise, centrifuged to precipitate F-actin, and the resulting pellet (P) and supernatant (S) fractions analysed by SDS-PAGE followed by Coomassie staining. Actin bands, indicated by solid arrow, are present in all lanes due to carry-over during sample loading. Aldolase bands are indicated by a dashed arrow. B) Supernatant and pellet fractions of a co-sedimentation assay similar to that shown in A. A fixed amount of actin was polymerised in the presence of increasing molar ratios of aldolase and samples were centrifuged. Resulting fractions were analysed by SDS-PAGE and western blotting with an anti-aldolase primary antibody. Aldolase-actin molar ratios are shown above the fractions from each sample. Approximate molecular weight is shown on the right of each gel or blot. Supernatant and pellet fractions derived from the same sample are vertically aligned.

** **Figure 2: Aldolase actin binding has reciprocal functional effects *in vitro*.** A) Falling-ball viscosity measurements of G- and F-actin samples in the presence of increasing molar ratios of aldolase. Numbers in () indicate the molar ratio of aldolase to actin monomers in each sample. (a) Denotes a significant difference compared to G-actin and (b) compared to F-actin (0) samples at $P<0.01$ using Student's, two-tailed, homoscedastic t-test. B) Aldolase specific activity in the presence of F-actin, G-actin, and BSA, at two different concentrations of fructose-1,6 bisphosphate. (a) denotes a significant difference compared to corresponding G-actin sample and (b) to corresponding BSA sample at $P<0.01$ using Student's, two-tailed, homoscedastic t-test. C) Michaelis-Menten curves of aldolase activity in the presence of increasing amounts of polymerised actin. 1 unit (U) of enzyme activity corresponds to a substrate conversion rate of 1 μmol min^{-1}. All values are the average of at least three technical replicates. Error bars are S.E.M. Experiments were repeated at least twice with reproducible results.

** **Figure 3: Distribution of aldolase:RFP and free RFP expressed in an Arabidopsis aldolase knockout genetic background in seedling root epidermal and hypocotyl cells imaged by CLSM.** A) Western blot on crude protein extracts from wild type (Col-0), aldolase knockout (*fba8-1*), and three independent aldolase:RFP expressing plants (ARFP1, 2, and 3) using an anti-aldolase primary antibody. Approximate molecular weights of 70kD and 40 kD (arrows) as estimated by comparison to a molecular weight marker are indicated. The Ponceau S stained membrane before probing with the anti-aldolase antibody is shown as a loading control. B) Free RFP and aldolase:RFP in root epidermal cells; C) Free RFP and aldolase:RFP in hypocotyl cells;

** **Figure 4: Investigating the correlation of aldolase:RFP and free RFP with GFP:Lifeact, and aldolase:RFP with free GFP in Arabidopsis guard cells using CLSM.** Maximal intensity z-series projections of guard cells co-expressing: A) GFP:Lifeact with aldolase:RFP; B) GFP:Lifeact with free RFP; and C) free, cytosolic GFP with aldolase:RFP; GFP fluorescence (GFP:Lifeact and free GFP) is pseudocoloured green, RFP fluorescence (aldolase:RFP and free RFP) is pseudocoloured magenta, co-localizing voxels in the merged images are shown in white. The PCC panel is a pseudocoloured image showing the Pearson's correlation coefficient of the co-expressed fluorophores in each pixel, with blue indicating low correlation and red indicating maximum correlation of the two fluorophores (see reference bar below images). D) Spatially averaged Pearson's correlation coefficient (PCC) of GFP:Lifeact with aldolase:RFP (GFPLA/ARFP) or with free RFP (GFPLA/RFP), and free GFP with aldolase:RFP (freeGFP/ARFP). Values are the spatially averaged co-efficient ± S.E.M calculated from a minimum of seven independent CLSM, z-stack image series (n=7) for each of the co-expressing lines.

** **Figure 5: FRET-FLIM measurements of GFP:Lifeact expressed in Arabidopsis guard cells and in tobacco leaf epidermal cells.** A) GFP:Lifeact expressed alone (GFP:Lifeact) and co-expressed with aldolase:RFP (GFP:Lifeact/ARFP) in Arabidopsis guard cells. Images are color-coded according to the lifetime (in ns) of GFP in each pixel, a reference bar with the range of

lifetimes is shown below the images. B) Average lifetime of GFP:Lifeact when expressed alone (GFPLA), or co-expressed with aldolase:RFP (ARFP/GFPLA) in Arabidopsis guard cells. C) Average lifetime of GFP:Lifeact expressed alone (GFPLA), co-expressed with aldolase:RFP (ARFP/GFPLA), or with free RFP (RFP/GFPLA) in tobacco leaf epidermal cells. Values are the average lifetime of nine independent images per line for both Arabidopsis and tobacco experiments, error bars are S.E.M. Three different images were taken from each of three leaves originating from different plants (n=9). Average lifetimes for each image were calculated from regions of interest that excluded lifetime values from the stomatal pore region (arrowheads in A), where strong auto-fluorescence would result in spuriously high lifetime values. (a) is significantly different from corresponding GFPLA and (b) is significantly different from the RFP/GFPLA at $P<0.01$ using Student's, two-tailed, homoscedastic t-test.

** **Figure 6: Distribution of actin in guard cells of *fba8-1*, aldolase:RFP complemented and wild type plants.** GFP:Lifeact expressed in: A) *fba8-1,* B) aldolase:RFP complemented, and C) wild type Col-0 Arabidopsis guard cells. Images are maximal intensity projections of z-stack confocal series. Comparable images were acquired from at least three different leaves per line, originating from different plants.

** **Figure 7: Schematic gene model of Arabidopsis aldolase *FBA8* (*At3g52930*) and isolation of an *FBA8* knockout line.** A) Schematic diagram of the *FBA8* gene. 5'- (box) and 3'- (box arrow) un-translated regions (UTRs) are shown in light grey. Exons are shown as dark grey boxes. Introns are shown as lines. The approximate insertion sites of the T-DNA insertions in lines *fba8-1* (used in this work), *fba8-2,* and *fba8-3*, are indicated with white arrowheads. B) Shows the results of an RT-PCR targeting the full-length mature transcript of the aldolase gene and of an RT-PCR on the same cDNA, but targeting a fragment of a ubiquitin transcript as a reference, in individual *fba8-1* plants, progeny of a segregating plant population. Numbers 1, 2, 3, and 4 denote individual heterozygous (1 and 2) and homozygous (3 and 4) plants. C) Is a western blot with an anti-cytosolic aldolase antibody on crude protein extracts from wild type Col-0 and homozygous *fba8-1* leaves. D) Crude protein extracts from roots and

leaves of wild type and *fba8-1* homozygous seedlings were assayed for total aldolase enzyme activity. Values are the average of two technical replicates from at least two biological samples (>20 seedlings per replicate) for each genotype. Error bars are S.E.M. * is significantly different from the corresponding Col-0 sample at $P<0.01$ using Student's, two tailed, homoscedastic t-test. The experiment was repeated twice with similar results.

****Figure 8: Leaf temperature of *fba8-1* during a humidity drop treatment.**
A) Leaf temperature was measured by infrared imaging. Plants were imaged at 80% relative humidity (RH) for fifty minutes. Humidity was decreased to 40% RH and plants were imaged for over two hours. The dashed line indicates the time point where humidity began to decrease. Leaf temperature was compared to Col-0 and aldolase:RFP expressing *fba8-1* plants. Ambient temperature was measured in parallel. Values are the average temperature of three different leaves from three different plants ($n=9$) per line, error bars are S.E.M. *Fba8-1* leaf temperature was found to be significantly different from Col-0 and aldolase:RFP after the drop in RH, using one-way ANOVA.

A

Reagent	Sample					
	F-actin		Aldolase		G-actin	
	P	S	P	S	P	S
Actin	+	+	-	-	+	+
Aldolase	+	+	+	+	+	+
Polymerisation buffer	+	+	+	+	-	-

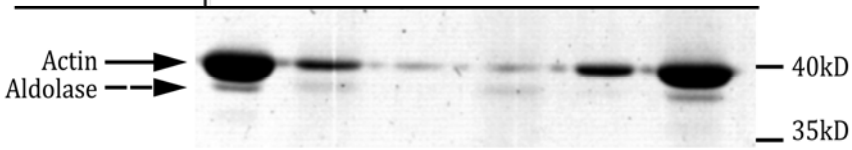

B

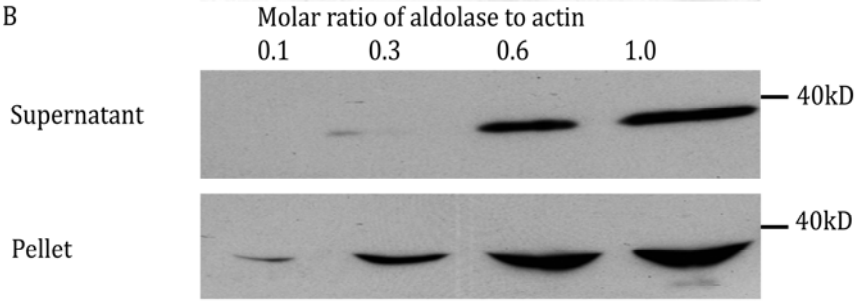

Figure 1

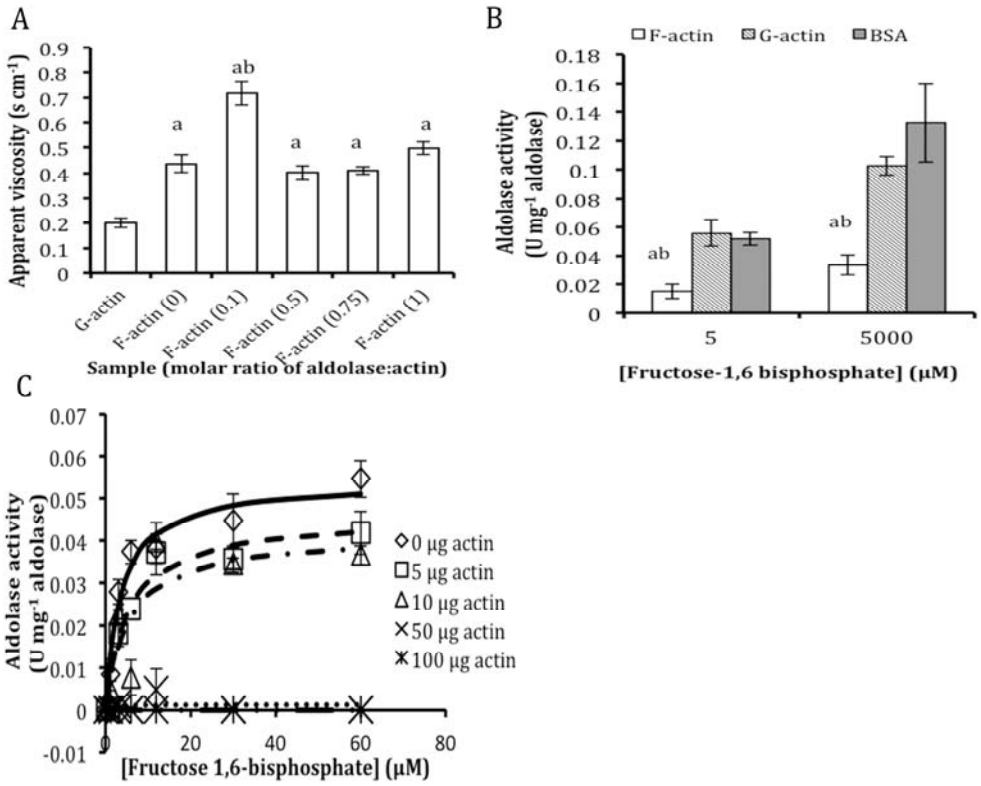
A
Apparent viscosity (s cm-1)
0.9
0.8
0.7
0.6
0.5
0.4
0.3
0.2
0.1
0
a
ab
a
a
a
G-actin
F-actin (0)
F-actin (0.1)
F-actin (0.5)
F-actin (0.75)
F-actin (1)
Sample (molar ratio of aldolase:actin)
B
F-actin
G-actin
BSA
Aldolase activity (U mg-1 aldolase)
0.18
0.16
0.14
0.12
0.1
0.08
0.06
0.04
0.02
0
ab
ab
5
5000
[Fructose-1,6 bisphosphate] (µM)
C
Aldolase activity (U mg-1 aldolase)
0.07
0.06
0.05
0.04
0.03
0.02
0.01
0
-0.01
0
20
40
60
80
[Fructose 1,6-bisphosphate] (µM)
0 µg actin
5 µg actin
10 µg actin
50 µg actin
100 µg actin

Figure 2

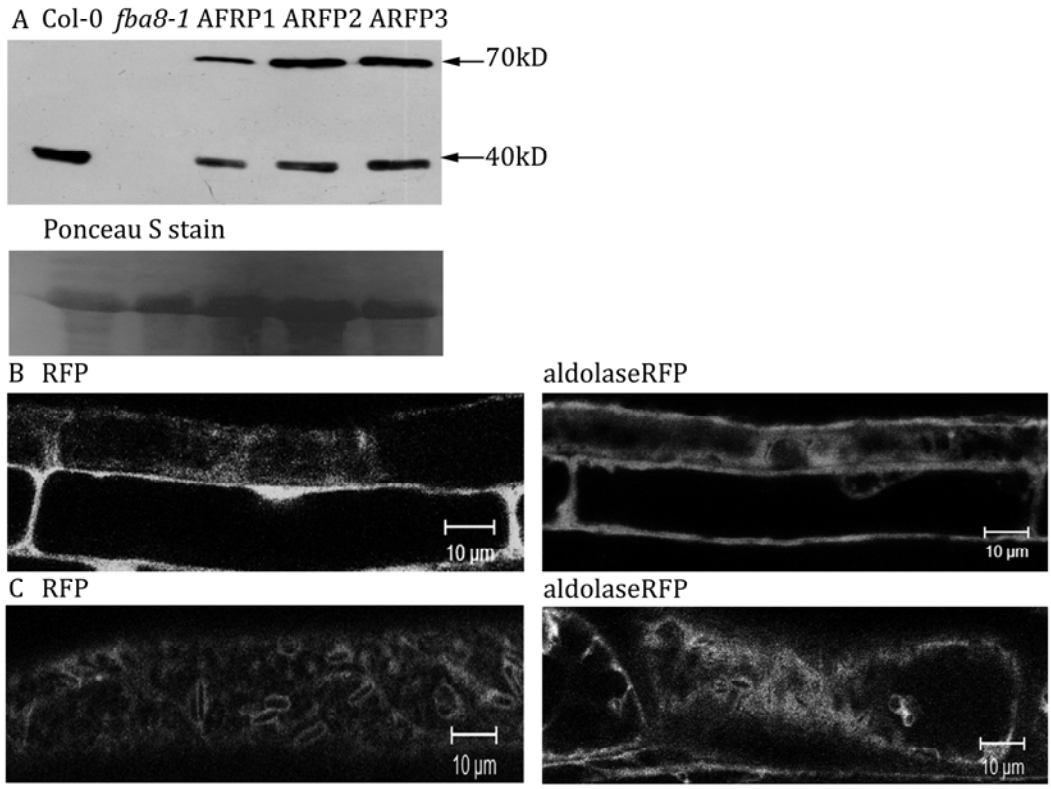
A Col-0 fba8-1 AFRP1 ARFP2 ARFP3
70kD
40kD
Ponceau S stain
B RFP
aldolaseRFP
10 µm
10 µm
C RFP
aldolaseRFP
10 µm
10 µm

Figure 3

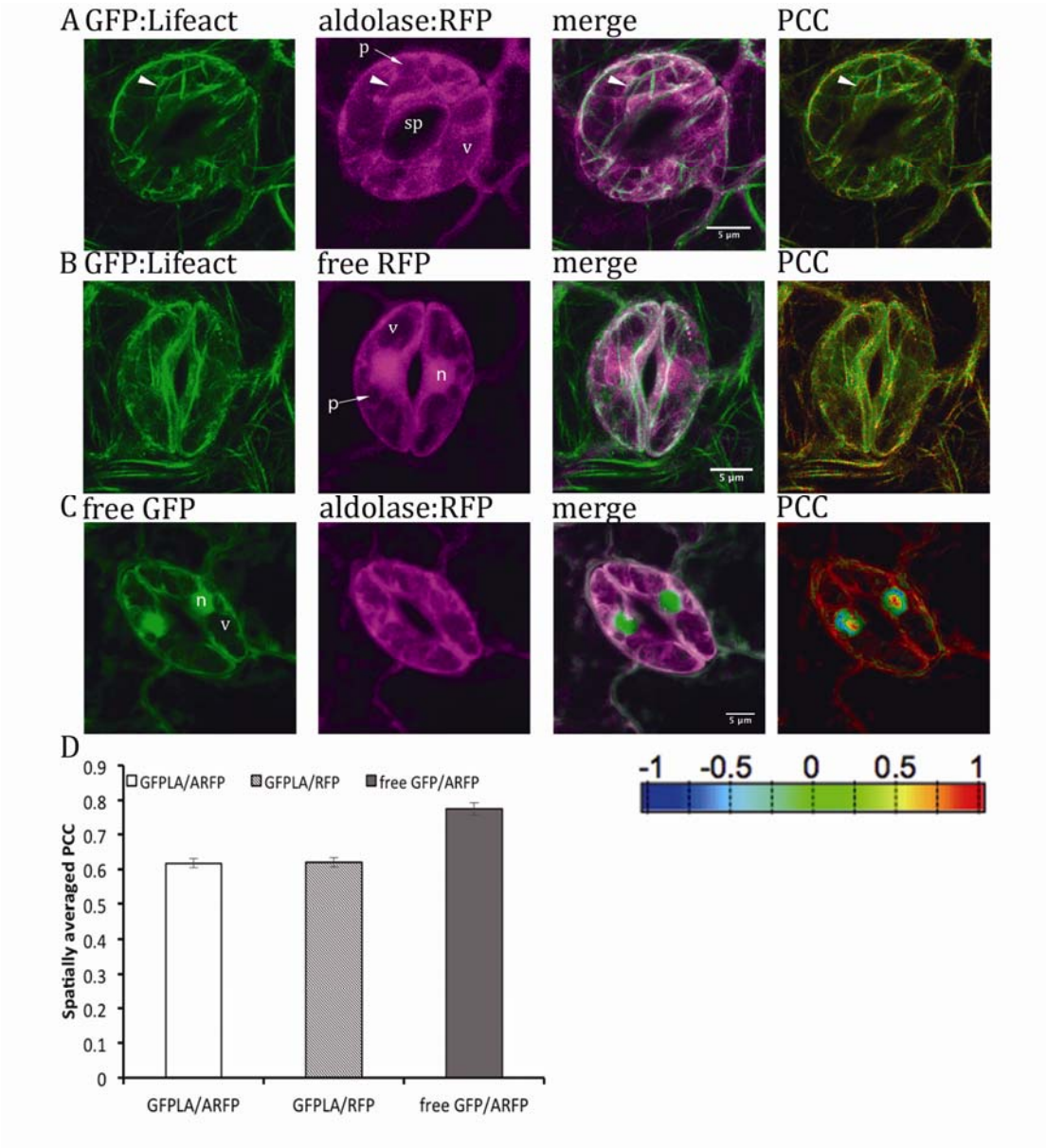
A GFP:Lifeact
aldolase:RFP
merge
PCC
p
sp
v
5 µm
B GFP:Lifeact
free RFP
merge
PCC
v
n
p
5 µm
C free GFP
aldolase:RFP
merge
PCC
n
v
5 µm
D
GFPLA/ARFP
GFPLA/RFP
free GFP/ARFP
Spatially averaged PCC
0.9
0.8
0.7
0.6
0.5
0.4
0.3
0.2
0.1
0
GFPLA/ARFP
GFPLA/RFP
free GFP/ARFP
-1
-0.5
0
0.5
1

Figure 4

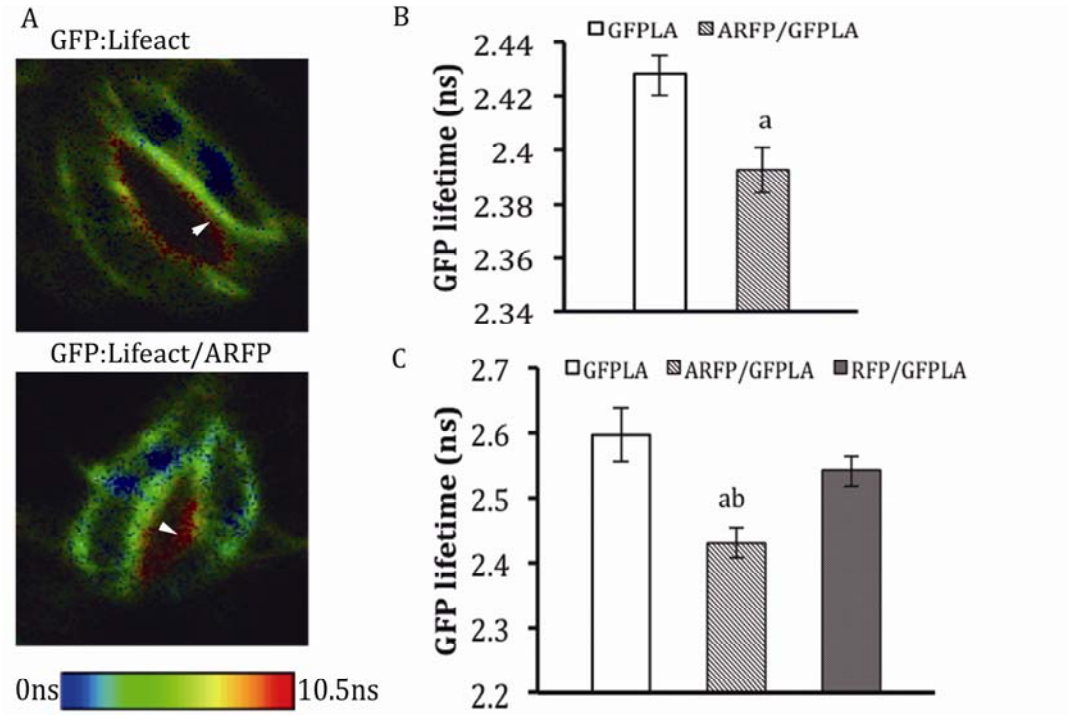
A
GFP:Lifeact
GFP:Lifeact/ARFP
0ns
10.5ns
B
GFPLA
ARFP/GFPLA
GFP lifetime (ns)
2.44
2.42
2.4
2.38
2.36
2.34
a
C
GFPLA
ARFP/GFPLA
RFP/GFPLA
GFP lifetime (ns)
2.7
2.6
2.5
2.4
2.3
2.2
ab

Figure 5

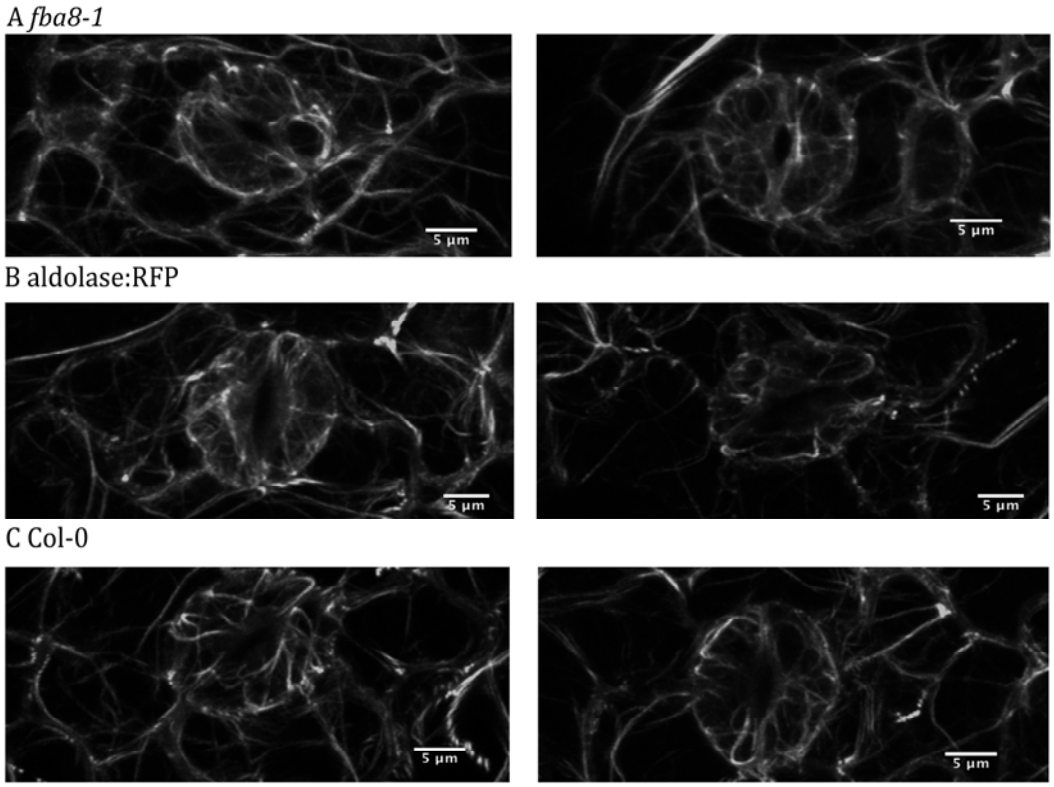

Figure 6

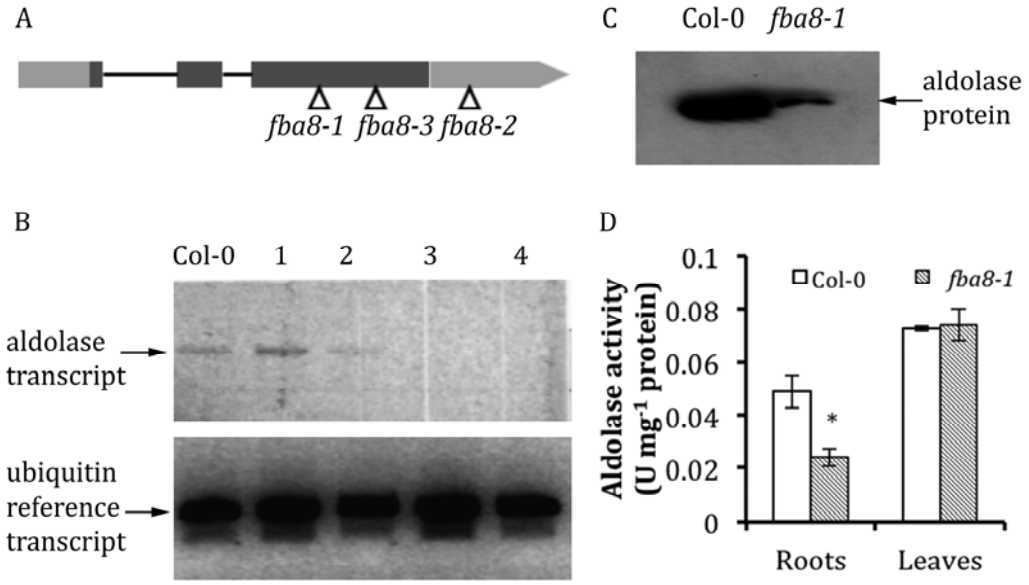
A
fba8-1
fba8-3
fba8-2
C
Col-0
fba8-1
aldolase protein
B
Col-0
1
2
3
4
aldolase transcript
ubiquitin reference transcript
D
Aldolase activity (U mg-1 protein)
0.1
0.08
0.06
0.04
0.02
0
Col-0
fba8-1
*
Roots
Leaves

Figure 7

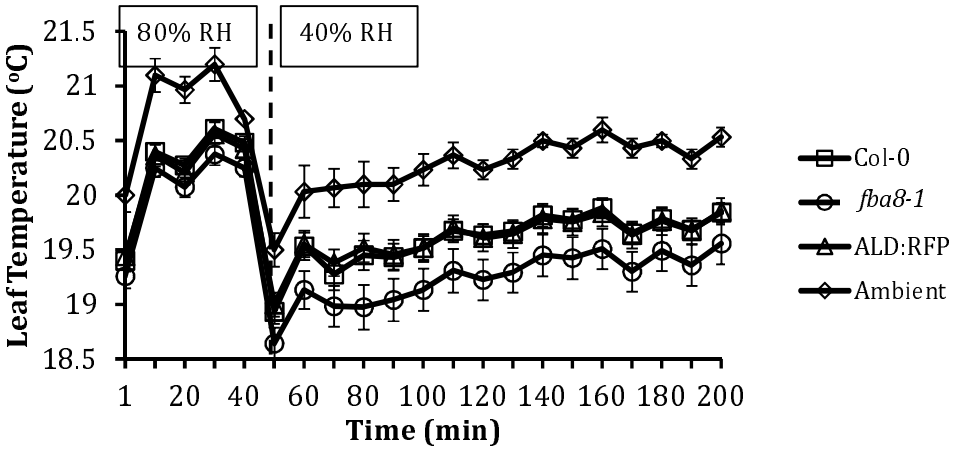
80% RH
40% RH
Leaf Temperature (°C)
21.5
21
20.5
20
19.5
19
18.5
1
20
40
60
80
100
120
140
160
180
200
Time (min)
Col-0
fba8-1
ALD:RFP
Ambient

Figure 8